Unmanned Systems, Vol. 1, No. 2 (2013) 177–198

DOI: 10.1142/S2301385013400025

UNMANNED SYSTEMS
http://www.worldscientific.com/worldscinet/us

Extractor X — Autonomous Tilt Rotor UAV

Joshua Jang En Chao*

Mechanical and Aerospace Engineering, Nanyang Technological University, 50 Nanyang Avenue, Singapore 639798

This paper looks into conceptualization, implementation and validation of the potential role that hybrid quad tilt rotor unmanned aerial vehicles (UAV) may undertake in the near future, especially so in military applications. A tilt rotor is designed, built and analyzed with wind tunnel data, theoretical calculations and flight log data. In addition, the paper will discuss the flight mechanics involved during its transition from hover to forward flight. As the tandem wing tilt rotor encompasses two unconventional designs, numerous mathematical models were developed in the design of the UAV.

Keywords: UAV; tilt rotor; tilt wing; Vertical Take-Off and Landing (VTOL); transition; tandem; autonomous; unconventional; UAVForge; Singapore Amazing Flying Machine Competition (SAFMC).

1. Introduction

There have been numerous developments in UAVs since 1950s when losing pilots over hostile territory started becoming a concern for countries. Since then, many countries have started their own UAV programs on fixed wing UAVs and rotary wing UAVs.[1] Fixed wing UAVs are excellent in endurance and stealth while rotary wing UAVs are capable of Vertical Take-Off and Landing (VTOL). Tilt rotor UAV is able to alternate between fixed wing configuration and rotary wing configuration by tilting its rotors. This enables it to tap on the advantages of both platforms above without adopting their disadvantages.

While tilt rotors have unique features that make them stand out compared to conventional aircrafts, they possess some inherent design shortcomings. In,[2] Meyer discussed on some of the potential causes of the failure of tilt rotors. In,[3] Lee gives a brief operational history of V-22 Osprey, discussing the flaws in the tilt rotor and accidents encountered. Chana and Sullivan[4] study into detail the tilt rotor's download effect and disadvantages it brings.

There are several studies that look into the fundamentals of tilt rotor design and presents findings that allow greater understanding in the field. Radhakrishnan and Schmitz study the effect of ground effect in.[5] Fejtek and Roberts investigate the effects of wind effect on a hovering tilt rotor in.[6] Rutherford *et al.* presents a detailed analysis of advantages and disadvantages of tilt wing in.[7] Force presented a technology study of a tandem wing tilt rotor in.[8]

The topic under study in this paper includes the design, development and testing of an autonomous quad tilt rotor UAV. The design encompasses a UAV capable of vertical takeoff, hover, transit and cruise in forward flight. This paper will discuss the problems faced by existing tilt rotors and generate solutions for them. It looks into harnessing the advantages of tilt rotor, tilt wing and tandem wings to develop an improved tilt rotor configuration.

Section 2 discusses the review of Tilt Rotor, reviewing tilt rotors, tilt wings and tandem wing configuration. Section 3 presents the platform design, focusing on aerodynamics, flight mechanics, tilt mechanism and autopilot. Section 4 describes the implementation of the platform design in wind tunnel testing, platform fabrication and tilt mechanism fabrication. Lastly, Sec. 5 presents the experimental results collected from experiments and flight testings.

Received 27 February 2013; Accepted 31 August 2013; Published 28 October 2013. This paper was recommended for publication in its revised form by Guest Editor, Stephen D. Prior.
Email Address: *joshuachaoje@gmail.com

Table 1. Comparison of UAV.

	TR 918 Eagle Eye	MQ-8B Fire Scout	RQ-7 Shadow	MQ-1 Predator
Class	Tactical, Tilt-rotor	Tactical, Helicopter	Tactical, Airplane	MALE, Airplane
Empty mass (kg)	590	940.3	84	512
Fuel mass (kg)	335	217.7	51.9	304
Payload (kg)	95	272	34.1	204
Gross mass (kg)	1020	1430	170	1020
Length (m)	5.56	7.3	3.4	8.22
Width/Span (m)	7.37	8.4	4.3	14.8
Height (m)	1.88	2.9	1	2.1
Max speed (m/s)	102.8	59.2	60.6	60.3
Cruise speed (m/s)	100	55.6	46.3	45.8
Loiter speed (m/s)	—	—	33.4	27.8
Radius of operation (km)	583.4	203.7	109	550
Endurance (h)	6	8	6	24
Service ceiling (km)	6.1	6.1	4.6	7.6
Power (kW)	427	313	28.3	86

2. Review of Tilt Rotor UAV Platforms

Tilt rotors exist in various forms, including twin, tri and quad configurations. Due to their ability to take off, land vertically and also cruise at high speeds, they have the capability of outperforming other UAV of their class.[9]

The Eagle Eye TUAV is compared to three other aircrafts chosen for their UAV class and gross take-off weight. The helicopter UAV taken for comparison is the MQ-8 Fire Scout, a tactical VTOL UAV used by the US Navy. The fixed wing UAVs chosen are the RQ-7 Shadow and MQ-1 Predator. The RQ-7 Shadow is a tactical UAV with similar endurance and flight altitude, whereas the MQ-1 Predator has the same take-off weight and operational range as the Eagle Eye.

Compared to all the three models, the Eagle Eye has the highest power output and is able to fly about twice as fast as any of the others. It also has an operational radius much larger than the two other tactical UAVs and similar to the MALE Predator. However, the Eagle Eye loses out in payload capability when compared to the Fire Scout or the same-weight Predator.

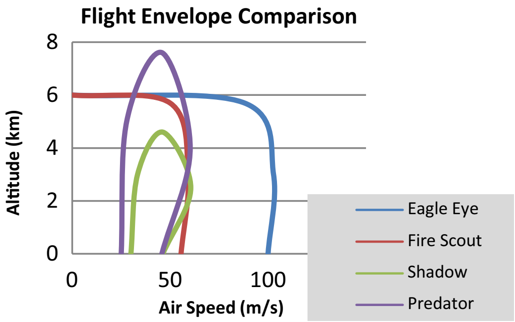

Fig. 1. Flight envelop comparison.[10]

A comparison of the flight envelope of the four aircrafts highlights the advantage of the Eagle Eye UAV and its versatility as shown in Fig. 1. Tilt rotors, like the Eagle Eye, are capable of covering a much wider range of speeds and different altitudes compared to the rest.[10] This makes the Eagle Eye a much rugged and versatile UAV that can be deployed in harsher environments and for more demanding missions.

2.1. *Twin tilt rotor*

The most common tilt rotor developed is twin tiltable rotors attached at the tip of the wings such as the Osprey V-22. However, they post numerous problems.

First, their efficiency is not able to match those of airplanes and helicopters. As their motors are mounted on wing tips, flexing of the wing must be prevented by strengthening the wing, which in turn increases the empty weight. To reduce that problem, wings are shortened, reducing the aspect ratio and thus lift to drag ratio. This results in a heavier aircraft affecting hover and short wingspan affecting cruise.

Second, twin tilt rotors are unstable at low speeds and when tilting between 35° and 80°, lead to numerous crashes and hard landings.[2] Xili *et al.* modeled the autonomous transition of V-1 and V-22. They identified nonlinear and redundant inputs that results in the complexity of the transition.[11]

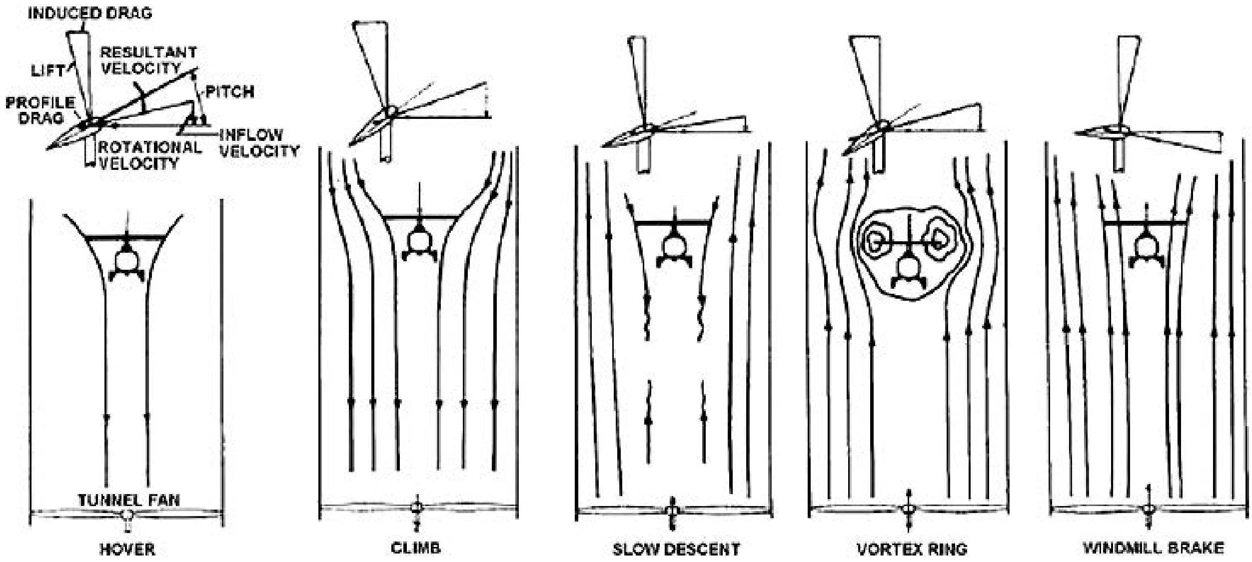

Fig. 2. Illustration of vortex ring state.

Third, the high-twist, high RPM blades in twin tilt rotors are needed to allow the two relatively small rotors to generate enough thrust to lift the aircraft. However, this results in a dangerous aerodynamic phenomenon — Vortex Ring State (VRS) where the rotor becomes enmeshed in its own downwash and loses lift, with thrust from the remaining rotor rolling the aircraft into an uncontrollable inverted dive. An illustration is shown in Fig. 2. This phenomenon occurs during rapid descent, which is required for ops plans of such vehicles. This led to a fatal crash of V-22 in 2000, killing 19 Marines on board.[3] A study on the optimization of composite tilt rotor used a mixed variational formulation based on exact intrinsic equations of motion for moving beams and a finite-state dynamic inflow theory. Effects such as extension-twist coupling, choice of layups, and cross-sectional geometry of the blade are significantly improved.[12]

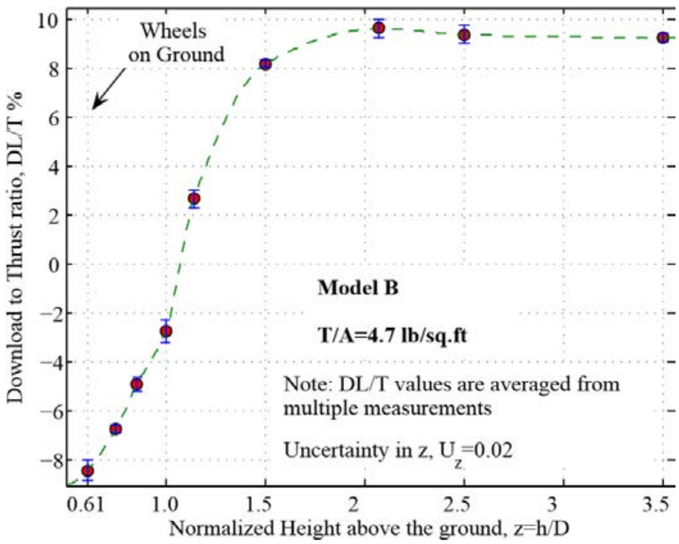

Fig. 3. Variation of download force with height.[5]

2.2. *Quad tilt rotor*

Quad tilt rotors have higher payload capabilities as compared to twin tilt rotor, but will require an additional wing and two more rotors, adding to its complexity.

During out of ground effect, download caused by downwash onto the wings is a major concern as it is significant and affects maximum payload capacity directly.[4,13] In one study, the download can go up to 9% of the thrust. However, during in ground effect, high pressure under the wings and fuselage cause an upload of 9% of the total thrust as the wake from four rotors meet underneath the fuselage and turned upward around the fuselage. The experimental data is shown in Fig. 3.[5]

In a study conducted by Fejtek and Roberts, computation by thin-layer Navier–Stokes equations shows that thin tangential jets from the leading edge is effective in decreasing the pressure in the upper surface, decreasing the effect of download.[6]

Another solution to reducing download is using the tilt wing concept. Compared to tilt rotors, tilt wing has lower download, better short take-off and landing and lower wing density required. However, it has less advantage in conversion flexibility.[7] A combination of tilt rotor and tilt wing is possible to tap on advantages of both configurations.

Quad Tilt Rotors are designed for heavy lifting of payload for transportation. Due to its ability to hover and carry out forward flight, it has its own unique mission profile as shown in Fig. 5.[8]

During the low-level delivery/Extraction segments, a low acoustic signature is desired. Casalino *et al.* successfully used a chain of computational method to predict the acoustic signature to improve airframe noise shielding effects.[14]

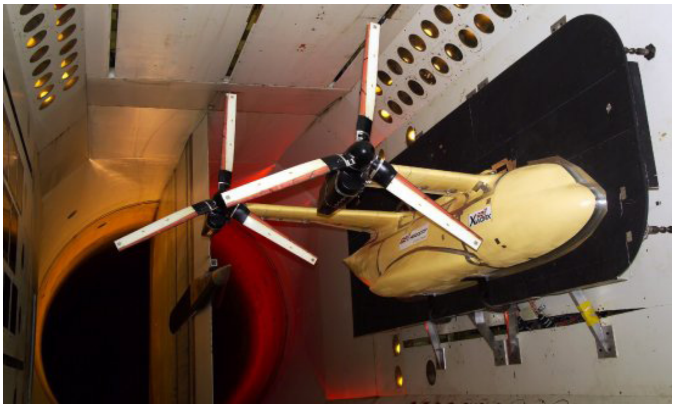

Fig. 4. Wind tunnel testing by Boeing.

2.3. *Tandem wing*

McGree and Kroo conducted a theoretical experiment and suggested that a tandem wing configuration is better optimized than conventional configurations.[15] Experiments from Calarese show that the flow from the front wing's leading edge separates and produce vortex sheets that roll up into vortices on the upper surface. This interferes with the turbulence characteristics of the rear wing resulting in increased lift and decreased trim drag.[16]

As both wings of a tandem wing are designed to produce lift, it is important to allow both wings to have laminar flow over its surface. Using k–ε turbulence model and CFD software, it is concluded that the wake of the leading airfoil

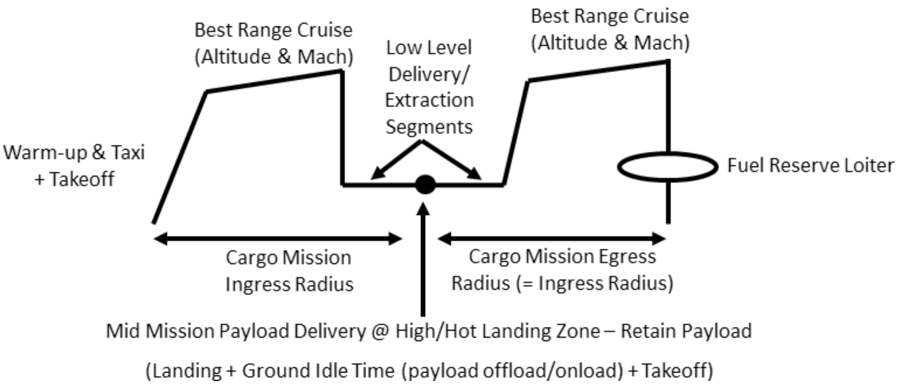

Fig. 5. Generic mission profile.[8]

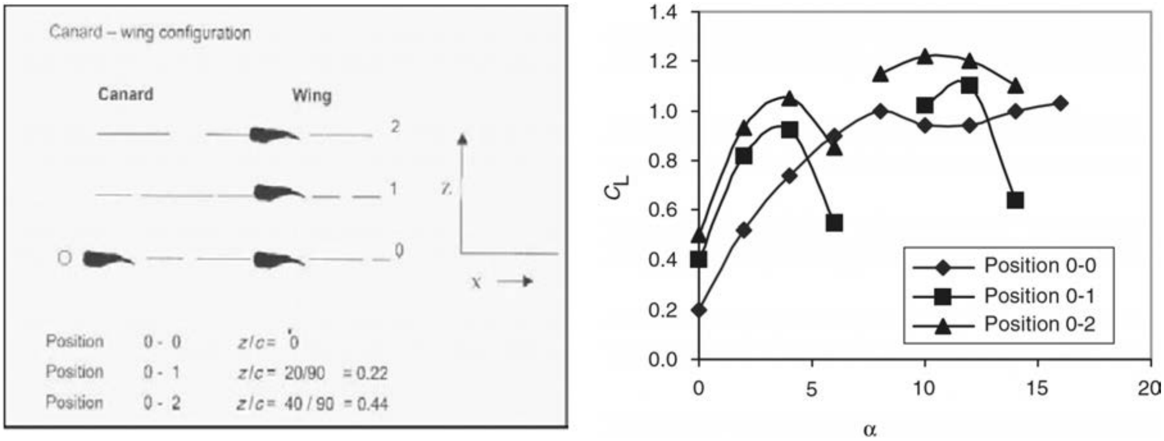

Fig. 6. Lift coefficient for different rear wing elevation.[17]

disturbs the inflow at the trailing edge. In an experiment, when the rear wing was elevated, the total lift coefficient increased significantly.[17]

3. Platform Design

3.1. *Aerodynamics*

Due to the unconventional and complex design of a tandem wing tilt rotor, aerodynamics must be studied for hover, transition and cruise.

3.1.1. *Hover*

The quad tilt rotor experiences download during OGE and upload during IGE due to the interaction between the propeller wash and the wings and fuselage. As most of the hovering is during OGE, it is important to reduce the download during OGE.

This can be achieved by designing the wing surface in the propeller flow to tilt together with the rotor, thus decreasing the surface area in the propeller wash. A down side to this is the susceptibility to gusts during hovering due to the tilted wing surface, reducing the stability of the UAV. As such, it is important to find a balance between the two scenarios and design an optimal tilt wing area.

A mathematical model is developed to determine the area of wings to tilt. This area is determined by prop size, prop wash angle and height of motor assembly. For motors mounted at the wingtips, with a half prop size of 10 cm and motor assembly height of 3 cm, Fig. 7 shows the length of tiltable wing required.

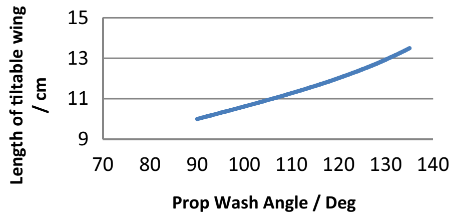

Fig. 7. Mathematical model for length of tiltable wing tip required.

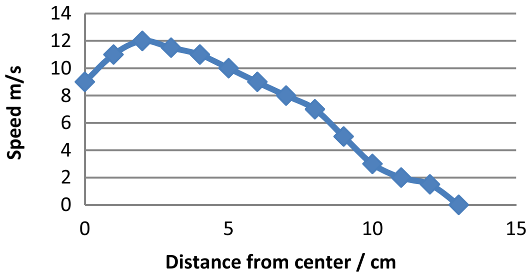

Fig. 8. Wind speed versus distance from propeller center.

This angle is experimentally determined using a pitot tube to measure regular intervals of wind velocity at a fixed distance of 12 cm away from the propeller. The change in wind speed is shown in Fig. 8.

Prop wash angle

$$= \tan^{-1}\frac{\text{null pitot reading} - \text{prop radius}}{\text{distance between prop and pitot tube}} + 90^\circ$$

$$= \tan^{-1}\frac{13-10}{12} + 90^\circ$$

$$= 104^\circ.$$

The propeller wash was determined to be 104°. According to Fig. 7, the minimum length of tiltable wing is about 10.9 cm. As such, the tiltable wing is designed to be 12 cm.

3.1.2. *Transition*

During transition, the rotors are tilted and the propellers create a wash on the wing where the rotors are attached. There is an additional wash on the rear wings from the front rotors, causing the rear wings to be more affected by the wash. This can be avoided by increasing the elevation of the rear wing such that the front propellers do not affect it.

For a propeller wash angle of 104°, the result shows that a rear tail with elevation of 10.92 cm and below will experience downwash; elevation between 10.92 and 24.88 cm will experience upwash and beyond 24.88 cm will experience no wash. The graph is shown in Fig. 10.

3.1.3. *Cruise*

Vortex Lattice Method (VLM) is a powerful tool to analyze inviscid flows around lifting bodies. However, the tandem tilt rotor travels at a cruise speed of 30 m/s giving a Reynolds number of only 4,000,000, causing the VLM method to be unrealistic. XFLR5 postulates that the viscous and inviscid contributions to aerodynamic forces are linearly independent, so that an inviscid VLM output may be complemented by a viscous XFoil analysis to get a more realistic mathematical model.[18]

The tandem tilt rotor uses NACA 2610 for both front and rear wings. Using XFLR5, the relationships between lift coefficient, drag coefficient, moment coefficient and angle of attack of the airfoil is determined for −2.0° and 7.0°. The relationships are shown in Fig. 11.

From Fig. 11, it can be seen that an angle of attack of 3° gives the highest lift to drag ratio of 105 for 2,000,000 Re.

After obtaining the results above, NACA 2610 was found to be most suitable for the tandem wing tilt rotor due to its peak L/D ratio and the angle of attack to achieve it.

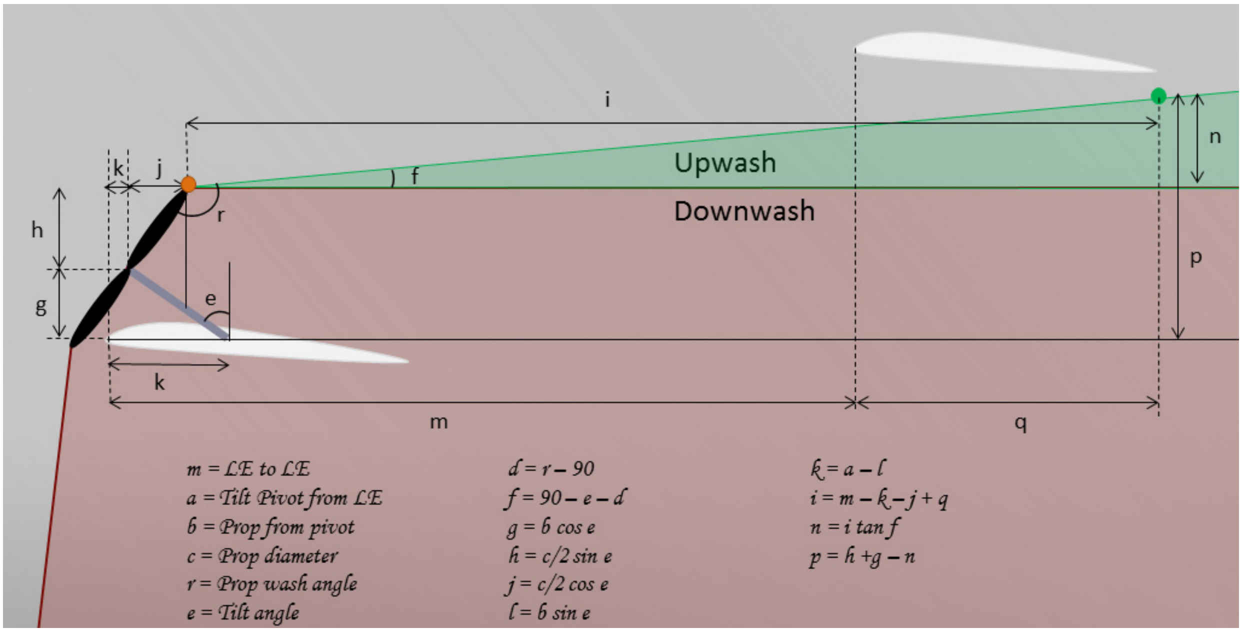

Fig. 9. Rear wing elevation determination to avoid downwash or upwash.

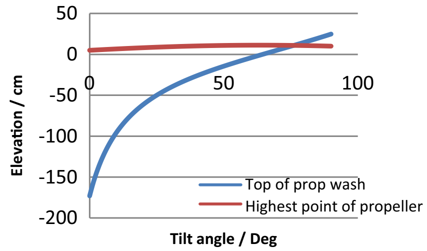

Fig. 10. Graph of rear wing elevation determination.

The NACA 2610 is used for both front and rear wings, and a 3D analysis of the wing configuration was investigated. The aim of the simulation is to determine a design that reduces interaction between the front and rear wings by varying the distance between the front and rear wings. Figure 12 shows CL versus AOA for varying distances.

It can be observed that as the rear wing is elevated, there is a significant increase in coefficient of lift for the particular angle of attack.

The relationships between lift coefficient, drag coefficient, moment coefficient and angle of attack of the tandem wing is determined for $-2.0°$ and $4.0°$ for the various combination. The simulation determined that option 3 provides sufficient clearance between the 2 wings in both *x*- and *y*- direction. The relationships are shown in Fig. 13.

3.2. *Flight mechanics*

3.2.1. *Model*

The model of the tandem wing tilt rotor is created and Figs. 14–16 show the basic forces and moments experienced during hover, transition and forward flight. There are additional forces such as downwash and also changing CG position, which will be discussed in detail.

3.2.2. *Transition moments*

During transition, many individual factors contribute to the change in moment as shown in Fig. 17. They are mainly lift from wings, thrust from motors, drag, downwash and pitching moment about the AC.

While each wing will encounter downwash from the propeller attached to it, the rear wing will encounter additional downwash from the front propeller. This causes a pitch up moment.

To account for all the moments during transition, a mathematical model is created to calculate and sum all the contribution to moments. During transition, the moments were designed to increase from 0 to 0.2 Nm to allow increase the angle of attack for forward flight. The designed pitch moment is shown in Fig. 18.

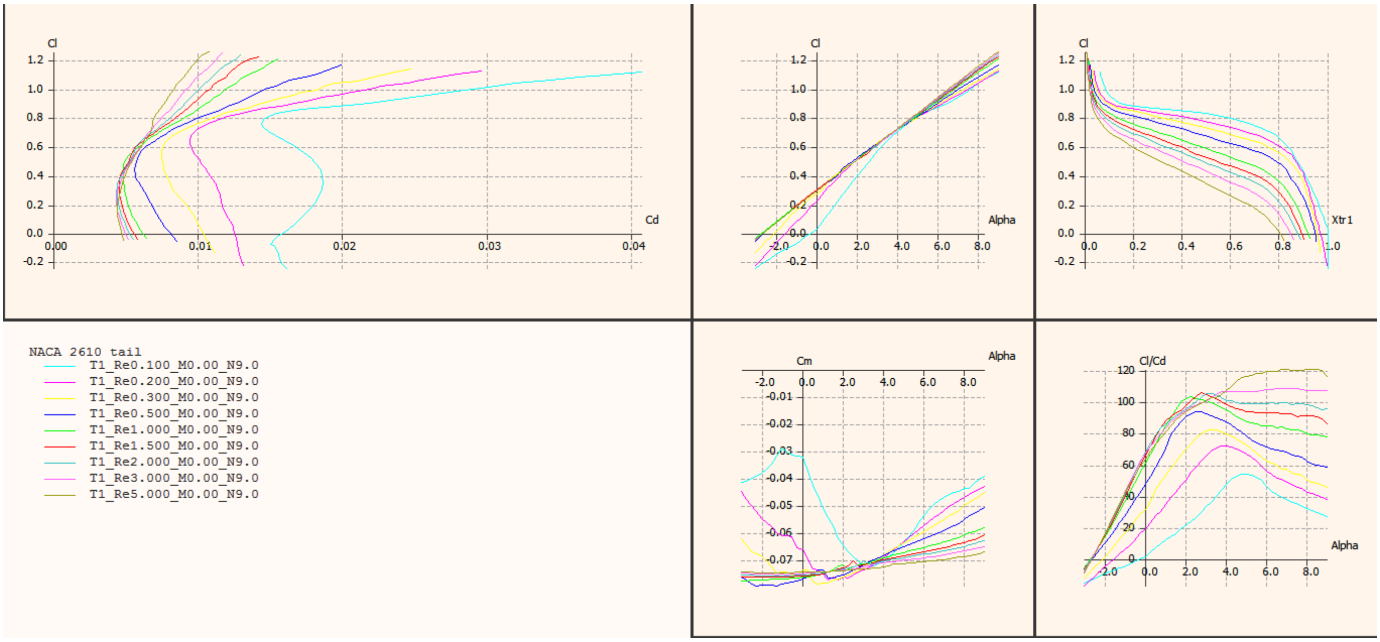

Fig. 11. Relationship of lift, drag and moment coefficient and angle of attack for 2D NACA 2610.

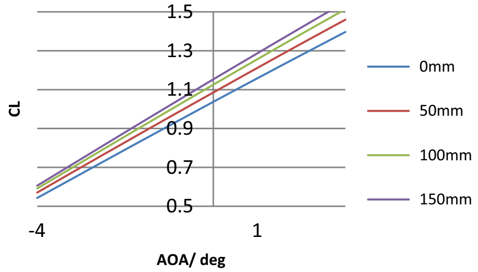

Fig. 12. CL versus AOA for varying rear wing elevation.

3.2.3. *Rate of transition*

During transition, the lift generation role is transferred from the motors to the wings. To ensure that the transition is smooth and executed at constant altitude, the maximum rate of tilting must be calculated based on various aerodynamic and physical constants. Figure 19 shows the region of tilting that enables smooth and constant altitude transition.

From the model, a constant tilt rate of 0.9°/s was designed which allows the whole transition to be carried out in 10 s.

3.2.4. *Stability and control*

Longitudinal Stability

The static margin is a concept used to characterize the static stability and controllability of aircrafts. The static margin in aft CG configuration needs to be between 5% and 8%.

$$SM = \frac{x_{NP}}{\bar{c}} - \frac{x_{cg}}{\bar{c}}. \tag{1}$$

The neutral point equation from Flight Stability and Control is only applicable to conventional aircraft with a wing and a tail.[19]

$$\frac{x_{NP}}{\bar{c}} = \frac{x_{cg}}{\bar{c}} - \frac{C_{m\alpha f}}{C_{L\alpha w}} + \eta V_H \frac{C_{L\alpha f}}{C_{L\alpha w}}\left(1 - \frac{d\varepsilon}{d\alpha}\right). \tag{2}$$

In order to calculate the neutral point of a tandem wing, the equation must be derived.

$$\begin{aligned}
C_{m_\alpha} &= C_{m_{\alpha w}} + C_{m_{\alpha f}} + C_{m_{\alpha t}} \\
C_{m_\alpha} &= C_{L_{\alpha w}}\left(\frac{x_{cg}}{\bar{c}}\right)_w - C_{L_{\alpha w}}\left(\frac{x_{ac}}{\bar{c}}\right)_w + C_{m_{\alpha f}} \\
&\quad + C_{L_{\alpha t}}\left(\frac{x_{cg}}{\bar{c}}\right)_t - C_{L_{\alpha t}}\left(\frac{x_{ac}}{\bar{c}}\right)_t, \\
C_{m_\alpha} &= C_{L_{\alpha w}}\left(\frac{x_{cg}}{\bar{c}}\right)_w - C_{L_{\alpha w}}\left(\frac{x_{ac}}{\bar{c}}\right)_w + C_{m_{\alpha f}} \\
&\quad + C_{L_{\alpha t}}\frac{-\left[\left(x_{LE_t} - x_{LE_w}\right) - x_{cg_w}\right]}{\bar{c}_t} - C_{L_{\alpha t}}\left(\frac{x_{ac}}{\bar{c}}\right)_t, \\
C_{m_\alpha} &= C_{L_{\alpha w}}\left(\frac{x_{cg}}{\bar{c}}\right)_w - C_{L_{\alpha w}}\left(\frac{x_{ac}}{\bar{c}}\right)_w + C_{m_{\alpha f}} \\
&\quad + C_{L_{\alpha t}}\frac{-\left(x_{LE_t} - x_{LE_w}\right) + x_{cg_w}}{\bar{c}_t} - C_{L_{\alpha t}}\left(\frac{x_{ac}}{\bar{c}}\right)_t,
\end{aligned}$$

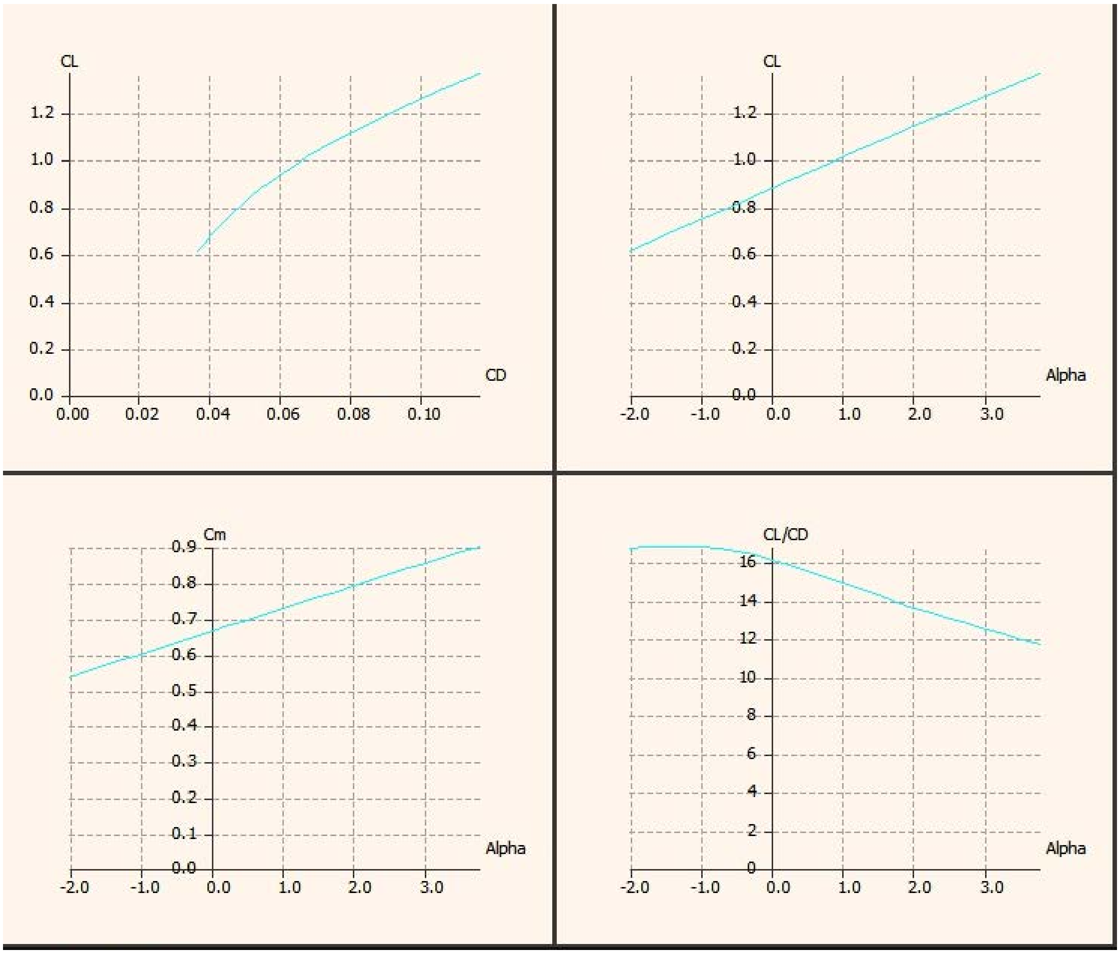

Fig. 13. Relationship of lift, drag and moment coefficient and angle of attack for tandem wing.

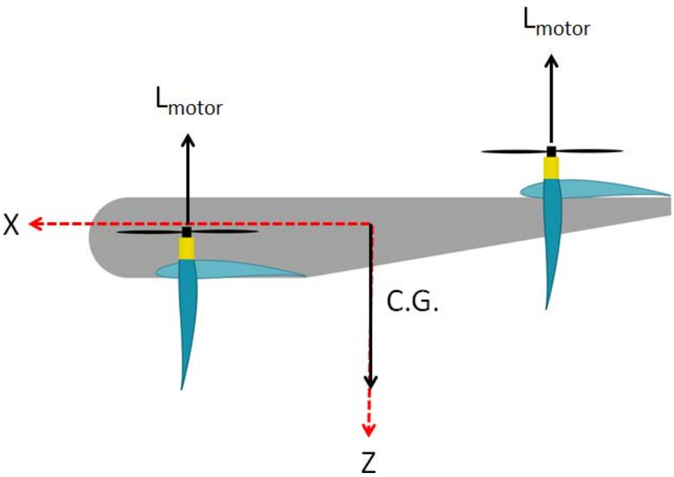

Fig. 14. Model during hover.

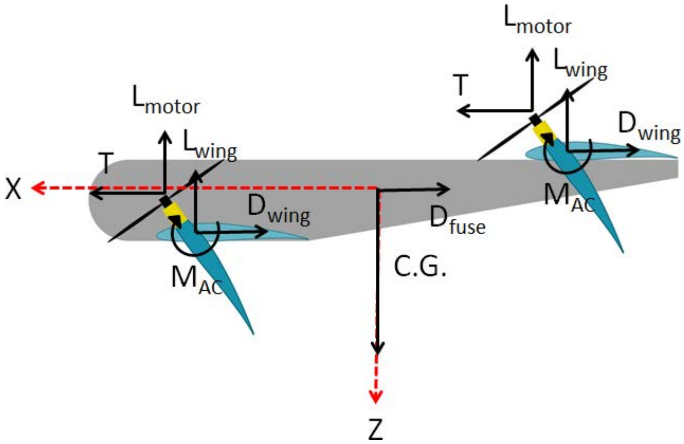

Fig. 15. Model during transition.

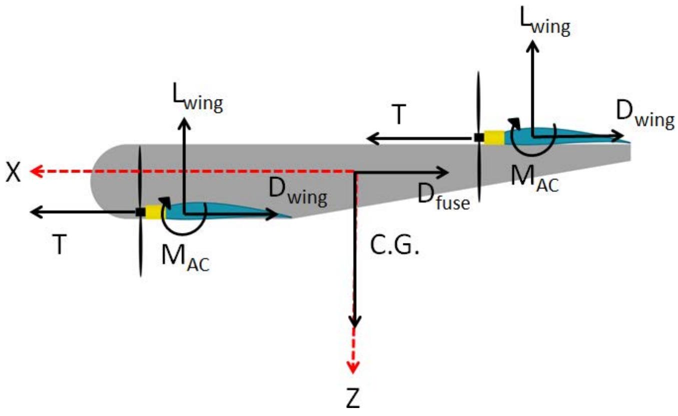

Fig. 16. Model during cruise.

$$C_{m_\alpha} = C_{L_{\alpha w}}\left(\frac{x_{cg}}{\bar{c}}\right)_w - C_{L_{\alpha w}}\left(\frac{x_{ac}}{\bar{c}}\right)_w + C_{m_{\alpha f}} - C_{L_{\alpha t}}\frac{x_{LE_t} - x_{LE_w}}{\bar{c}_t} + C_{L_{\alpha t}}\left(\frac{x_{cg}}{\bar{c}}\right)_w - C_{L_{\alpha t}}\left(\frac{x_{ac}}{\bar{c}}\right)_t.$$

Setting C_{m_α} equal to 0 and solving for the center of gravity position yields

$$C_{L_{\alpha w}}\left(\frac{x_{cg}}{\bar{c}}\right)_w + C_{L_{\alpha t}}\left(\frac{x_{cg}}{\bar{c}}\right)_w = C_{L_{\alpha w}}\left(\frac{x_{ac}}{\bar{c}}\right)_w - C_{m_{\alpha f}} + C_{L_{\alpha t}}\frac{x_{LE_t} - x_{LE_w}}{\bar{c}_t} + C_{L_{\alpha t}}\left(\frac{x_{ac}}{\bar{c}}\right)_t,$$

$$x_{cg_w} = \frac{C_{L_{\alpha w}}\left(\frac{x_{ac}}{\bar{c}}\right)_w - C_{m_{\alpha f}} + C_{L_{\alpha t}}\frac{x_{LE_t} - x_{LE_w}}{\bar{c}_t} + C_{L_{\alpha t}}\left(\frac{x_{ac}}{\bar{c}}\right)_t}{\frac{C_{L_{\alpha w}}}{\bar{c}_w} + \frac{C_{L_{\alpha t}}}{\bar{c}_t}},$$

$$x_{NP} = \frac{C_{L_{\alpha w}}\left(\frac{x_{ac}}{\bar{c}}\right)_w - C_{m_{\alpha f}} + C_{L_{\alpha t}}\frac{x_{LE_t} - x_{LE_w}}{\bar{c}_t} + C_{L_{\alpha t}}\left(\frac{x_{ac}}{\bar{c}}\right)_t}{\frac{C_{L_{\alpha w}}}{\bar{c}_w} + \frac{C_{L_{\alpha t}}}{\bar{c}_t}}. \quad (3)$$

The pitching moment contributes significantly to the longitudinal stability. For a plane to be longitudinally stable, it must provide a restoring pitching moment when subjected to disturbance in the longitudinal direction, in order to bring it back to equilibrium. The total pitching moment is obtained for the contribution from wing, fuselage and tail.

For a plane to be stable, the pitching moment slope must be negative. This is achieved by giving the front wing a higher angle of attack compared to the rear wing and deflecting the elevators slightly downwards to create a higher camber airfoil. This will move the CG forward from the center point, giving the rear wings a larger moment arm to enable a negative pitching moment. In addition, when the UAV pitches up, a higher camber airfoil will enable the front wing to stall first, causing a negative pitching moment. It will cause the UAV to return to a lower angle of attack, regaining airflow over the wings instead of causing both wings to stall.

A summary of the pitching moment slope is shown in Table 2.

Directional Stability

The plane can be considered to be directionally stable if it is able to produce a restoring yawing moment to return to its equilibrium position. The directional stability is mainly affected by the fuselage and the vertical fin. For a plane to have directional stability, the overall yawing moment slope must be positive. The fuselage produces a destabilizing effect and the fin produces a stabilizing effect. The yawing moment curve slope is shown in Table 3.

Lateral Stability

A plane is laterally stable if it can produce a restoring rolling moment when subjected to forces causing it to be

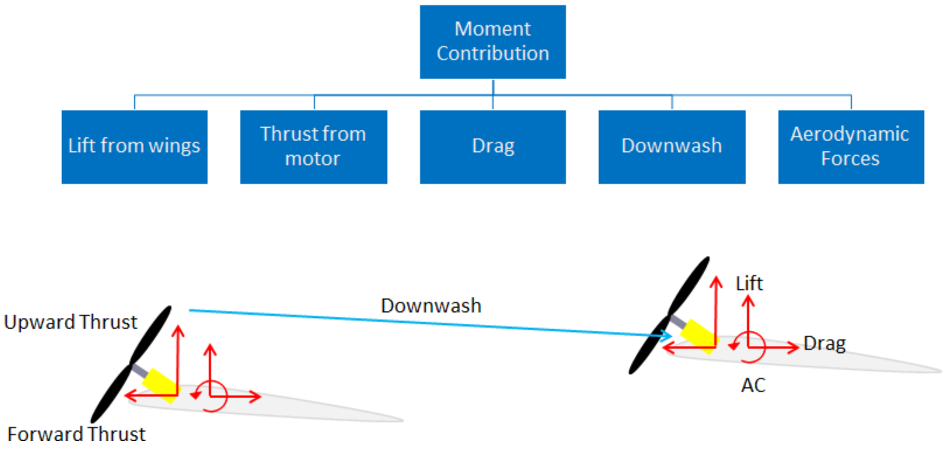

Fig. 17. Factors contribution to moments during transition.

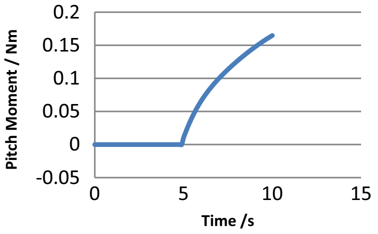

Fig. 18. Pitching moment versus time obtained from dynamic model.

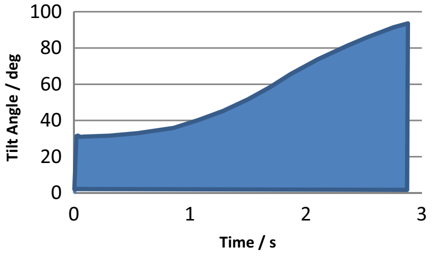

Fig. 19. Tilt rate region.

out of equilibrium position. The lateral stability is affected by geometrical dihedral, dihedral effect due to the wing's vertical placement and dihedral effect of sweep.

Even without geometrical dihedral, the sweep and vertical placement of the wing creates an effective dihedral effect. The wing and fin also provides lateral stability, resulting in an overall negative rolling moment curve slope. Table 4 shows various contributions to roll moment slope.

Table 2. Contribution of pitch moment curve slope.

Pitching Moment Curve Slope	/Rad
Wing contribution, $C_{m\alpha\text{wing}}$	5.70
Fuselage contribution, $C_{m\alpha\text{fuse}}$	0.016
Tail contribution, $C_{m\alpha\text{tail}}$	−6.77
Total, $C_{m\alpha}$	−0.91

Table 3. Contribution of yaw moment curve slope.

Yawing Moment Curve Slope	/Rad
Fuselage contribution, $C_{n\beta\text{fus}}$	−0.604
Fin contribution, $C_{n\beta v}$	0.22
Total, $C_{n\beta}$	0.21

Table 4. Contribution of rolling moment curve slope.

Rolling Moment Curve Slope	/Rad
Sweep contribution, $C_{l\beta w}/C_L$	−0.05
Geometrical dihedral, $(C_{l\beta})_\Gamma$	0
Vertical placement, $C_{l\beta wf}$	−0.0880
Wing contribution, $C_{l\beta w}$	−0.0115
Fin contribution, $C_{l\beta v}$	0.0624
Total, $C_{l\beta}$	−0.0525

Trim at CLmax at forward CG

Trim is defined as the state where moment equals zero. CLmax occurs at 0.1 rad AOA. From Fig. 20, an elevator deflection of 8° is required for trim at CLmax.

Trim at CLmax at aft CG

From Fig. 21, an elevator deflection of 0° is required for trim at CLmax.

Control surface sizing

The control surfaces are sized based on their ability to provide adequate control power for the most demanding maneuver during a flight routine.

Trim analysis is conducted to analyze whether the angle elevators deflection are sufficient to provide longitudinal

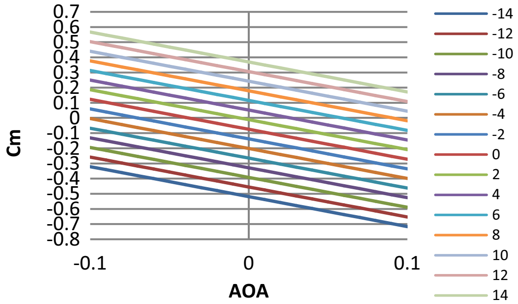

Fig. 20. Cm versus AOA at forward CG for different elevator deflections.

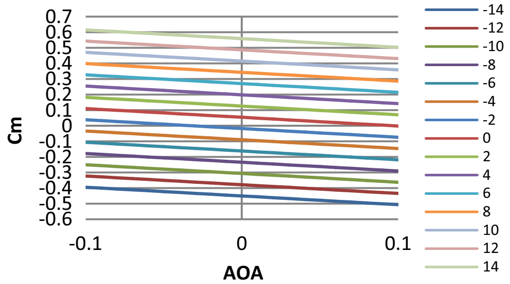

Fig. 21. Cm versus AOA at forward CG for different elevator deflections.

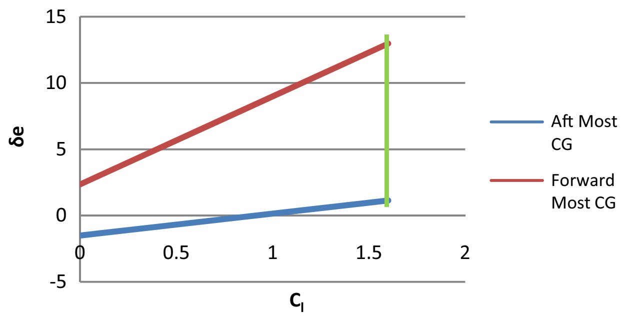

Fig. 22. Operating regime for trim.

control for both aft most CG and forward most CG conditions before CLmax. Elevator deflection was plotted against CL for both cases and the CLmax line is included. The enclosed area shown in Fig. 22 is the operating regime for trim flights. The maximum elevation deflection required is $+13°$, which is within the $+25°$ to $-25°$ limits.

The elevator control power of tandem wings is different from conventional fixed wings. Thus, the elevator control power must be derived as seen below.

$$\Delta C_m = \Delta C_{L_w}\left(\frac{x_{cg}}{\bar{c}} - \frac{x_{ac}}{\bar{c}}\right) = \left(\frac{x_{cg}}{\bar{c}} - \frac{x_{ac}}{\bar{c}}\right)_w \frac{dC_{L_w}}{d\delta_e}\delta_e, \quad (4)$$

$$C_{m_{\delta e}} = \left(\frac{x_{cg}}{\bar{c}} - \frac{x_{ac}}{\bar{c}}\right)_w \frac{dC_{L_w}}{d\delta_e} = \left(\frac{x_{cg}}{\bar{c}} - \frac{x_{ac}}{\bar{c}}\right)_w \frac{dC_{L_w}}{d\alpha_w}\tau$$
$$= \left(\frac{x_{cg}}{\bar{c}} - \frac{x_{ac}}{\bar{c}}\right)_w C_{L_{\alpha w}}\tau. \quad (5)$$

The parameters of the elevator and aileron are shown in Tables 5 and 6.

Table 5. Elevator parameters.

Elevator Authority	
Elevator area	0.0176 m^2
Elevator control power, $C_{m\delta e}$	1.99 rad^{-1}

Table 6. Aileron parameters.

Aileron Authority	
Aileron area	0.0176 m^2
Aileron control power, $C_{l\delta a}$	0.193 rad^{-1}

3.3. *Tilt mechanism*

The tilt-rotor actuators in existing tilt-rotor aircrafts, such as the V-22, include a complex system of bearings and supports, dual brakes, and screw travel-stops. As pylon position affects normal fights of tilt-rotors directly, detailed calculation of loads on the actuators is important to ensure reliability and performance. While manned tilt-rotors aircrafts have double redundancies for actuators, for the purpose of this project, safety factor for loading will be considered to reduce the probability of failure in flight.

While reliability is the most important factor in the tilt rotor mechanism design, other factors must be considered as the presence of four such mechanisms in a quad tilt rotor contributes significantly to weight and aerodynamic drag. Four main considerations were identified for the design of the tilt rotor mechanism of the quad tilt rotor UAV.

(1) The mechanism has to prevent rotation in any axis other than the actuator's designed axis of rotation (*Z*-axis).
(2) The mechanism must have minimal friction along its axis of rotation.
(3) The weight of the system must be kept to a minimum.
(4) The system's contribution to aerodynamic drag must be kept to a minimum.

Throughout the course of the project, three different tilt mechanisms were designed.

Direct Mounting

The direct mounting method requires the least amount of material and design complexity. It comprises a simple L-shaped mount where one side is mounted to the actuator and the other side mounted with the motor shown in Fig. 24.

Moment Arm

The moment arm method uses a moment arm attached to actuator. The design includes a mount, with the motor mounted on one of its surfaces. On the vertical surface, the mount is pivoted onto the airframe structure using a bolt and nut to restrict the rotation to the *Z*-axis. On the same

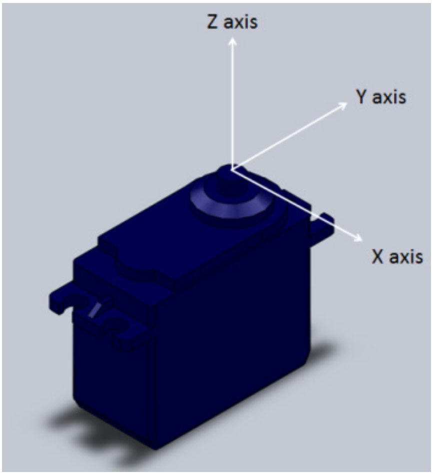

Fig. 23. Axis of actuator.

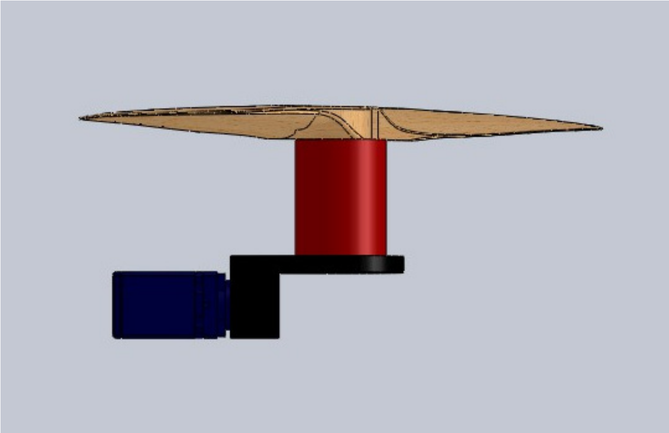

Fig. 24. Tilt mechanism — Direct mounting.

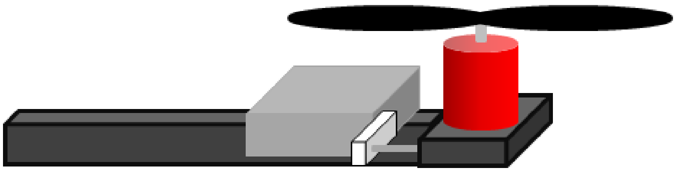

Fig. 25. Tilt mechanism — Moment Arm.

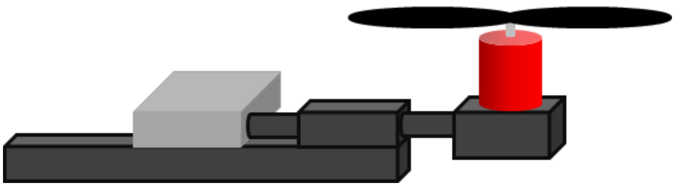

Fig. 26. Tilt mechanism — Torque Tube.

surface, there is a linkage with the actuator's moment arm, allowing the actuator to rotate the mount.

Torque Tube

The torque tube method is a combination of the above two concepts. The motor mount is connected to the actuator, similar to the direct mounting method, except it is via a carbon fiber tube. A carbon fiber guide maintains the position of the tube, only allowing rotation in the *Z*-axis.

Table 7 shows the comparison between the three different tilt mechanisms based on the considerations prescribed. This is based on a maximum motor thrust of 10 N and motor weight of 1 N.

For the final design, main contributions to the loads on the actuator are moment from the motor's mass and vibration of the motor.

Table 7. Comparison between different tilt mechanisms.

	Direct Mounting	Moment Arm	Torque Tube
Moment in *X*-axis	0.4 Nm	0 Nm	0 Nm
Moment in *Y*-axis	0.3 Nm	0 Nm	0 Nm
Moment in *Z*-axis	0.3 Nm	0.3 Nm	0.3 Nm
Actuator rating required	1.4 Nm	0.7 Nm	0.4 Nm
Area contributing to drag	30 cm^2	12 cm^2	0 cm^2
Weight	10 g	20 g	5 g

3.4. *Autopilot*

Various autopilots were considered and Ardupilot Mega was chosen due to its low cost and expandability. The open sourced Arducopter code supports only multicopters and the functions in red must be added to support the tandem wing tilt rotor.

Variable tilt angle function was also added into the autopilot.

4. Implementation of Platform Design

4.1. *Aerodynamics*

In order to understand and study the lift curve slope and lift to drag ratio for theoretical calculation of performance, wind tunnel testing was required. A 1/2.6th scaled model of Prototype I was constructed and tested in the low speed wind tunnel in Nanyang Technological University, School of Mechanical and Aerospace Engineering. Wind tunnel data was taken from 17 speeds between 4.3 and 14.9 m/s at an interval of 0.6 m/s. 20 angles were taken between $-5°$ and $14°$.

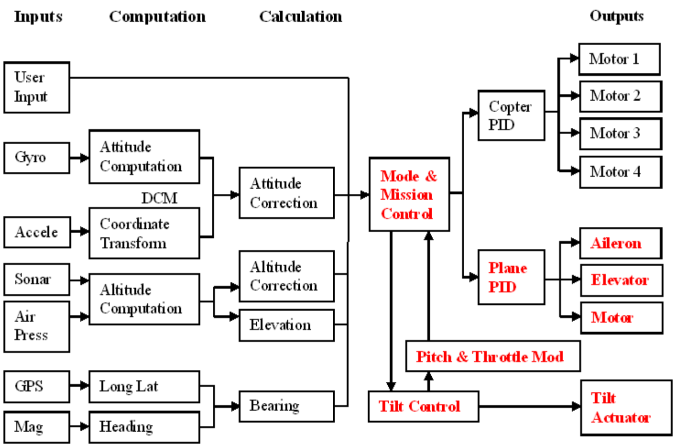

Fig. 27. Block diagram of operation.

Fig. 28. Wind tunnel setup.

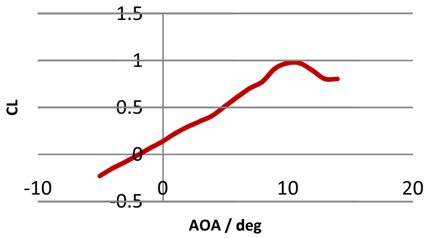

Fig. 29. Lift coefficient.

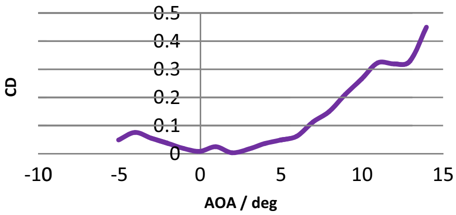

Fig. 30. Drag coefficient.

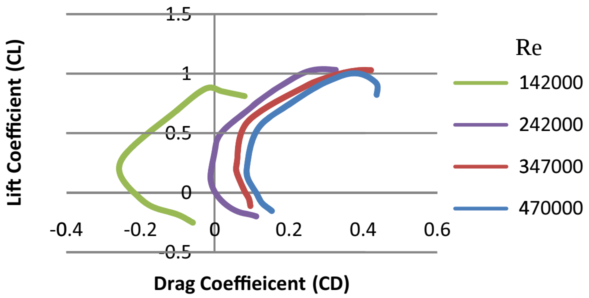

Fig. 31. CL versus CD.

From the data, CL = 0.13 at zero angle of attack. CD is the least at 2° angle of attack. These data will be used in the transition model to calculate the optimal tilt rates for transition.

4.2. *Platforms*

In the process of development, seven versions of the tilt rotor are designed, built and tested.

4.2.1. *Conventional plane with four rotors*

The first prototype developed is a merge between a conventional fixed wing and a quadcopter. In addition, tilt mechanisms are added to each rotor to allow transition. The purpose of using a conventional fixed wing is to add the quadcopter and tilt mechanism to a well-tested platform, in order to learn the interactions between quadcopter, tilt function and the flying platform in a structured manner.

This prototype worked well in hover, proving no adverse interaction by wing and tail in hover mode. However, due to the downwash from the rear rotors on the horizontal tail, it causes a pitch up moment during transition, bringing the plane into a loop.

Fig. 32. Prototype I.

4.2.2. *Tandem wing Prototype II & III*

The tandem quad tilt rotor has an advantage of additional lift and ability to embed the struts holding the rotors into the wings. This will allow increase in payload capacity and improving the aerodynamics of the UAV.

However, due to the use of a tandem wing, additional calculations and simulations are required as the tandem

Fig. 33. Prototype II.

Fig. 34. Prototype III.

wing design is not widely studied and the dynamics are much more complex. This is the reason for detailed analysis in aerodynamics and flight mechanics required in the design process.

To improve yaw damping, winglets are added to the design.

4.2.3. *Tandem wing prototype IV*

With the success of prototype III, a small version was designed and built for Singapore Amazing Flying Machine Competition. Prototype IV performed well and achieved second place in Cat E Unconventional category.

4.2.4. *Tandem wing prototypes VI and VII*

Prototype VI is an optimized version from the previous designs. It has improved endurance, range, efficiency and

Fig. 35. Prototype IV.

Fig. 36. Prototype VI.

portability. Prototype VI was submitted for UAVForge Competition, an international competition organized by DARPA.

After successful flight tests, the tilt rotor was professionally designed and fabricated.

Prototype VI achieved top 12 positions in all three milestones in UAVForge and was selected by USA government agency to attend the finals in Fort Stewart, USA in May 2012. The overall position during the finals was 6th.

4.3. ***Tilt mechanism***

The tilt mechanisms for all three versions were fabricated.

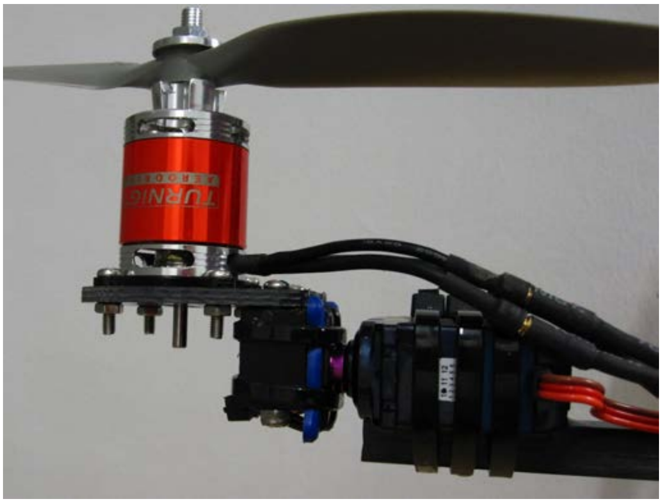

Fig. 37. Direct mounting.

4.3.1. *Direct mounting*

An L-shaped mount made of delrin is used to support the motor. The servo horn is mounted onto the delrin block to control the tilting of the motor. This method proves to be simple and effective. However, a 60 g servo with 1.4 Nm torque rating was used as the forces on the servo were great. In addition, the frontal area will cause significant drag during cruise.

4.3.2. *Moment arm*

The moment arm method uses two metal mounts to allow the motor to be pivoted onto a screw instead of the servo.

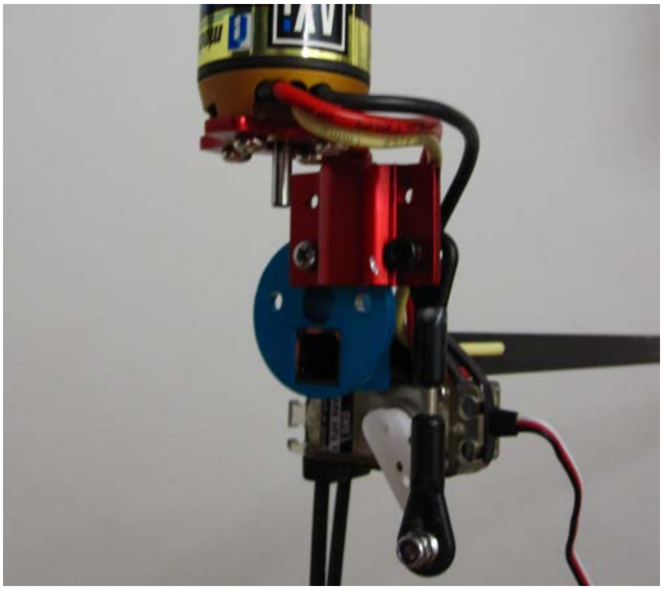

Fig. 38. Moment Arm.

Fig. 39. Torque Tube.

This reduces the servo weight required to 40 g. However, the weight of the mounts and push rods are significant and the complex design creates multiple possible points of failure.

4.3.3. *Torque tube*

The torque tube method attaches a carbon fiber tube directly to the servo. A hollow square rode acts as a guide to hold the tube in position and provides support, reducing stress on the servo. The motor and tiltable wing assembly is then attached to the end of the tube.

5. Flight Test Data

5.1. *Data logging*

Flight test in stabilized mode was conducted to investigate the Prototype VI's stability, maneuverability and performance. Numerous data were logged in the 16 MB flash memory at 50 Hz. The various data logged are shown in Table 8. The data logged are plotted and shown in Figs. 40 to 43.

Table 8. Customized data logged.

Time	Input	Output	GPS	Raw	Attitude
Milliseconds	Roll Pitch Yaw Throttle	Motor 1 Motor 2 Motor 3 Motor 4	Latitude Longitude Altitude Speed Course	Gyro *x, y, z* Acce *x, y, z*	Roll Pitch Yaw

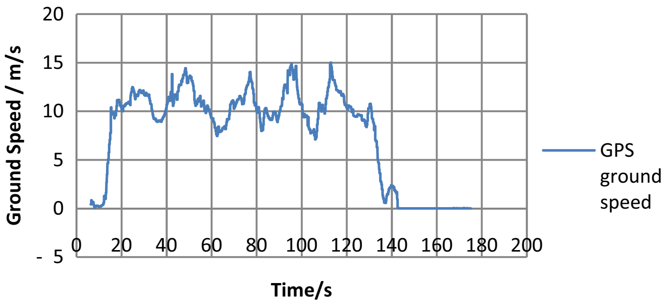

Fig. 40. GPS ground speed versus time.

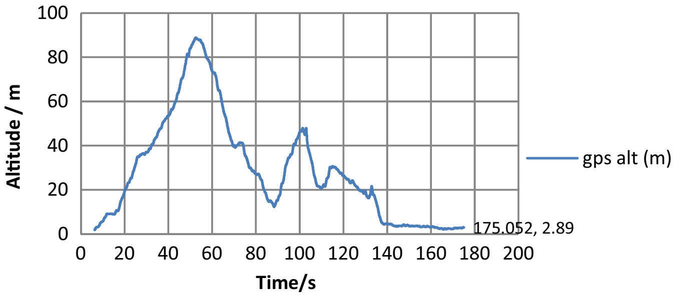

Fig. 41. GPS altitude versus time.

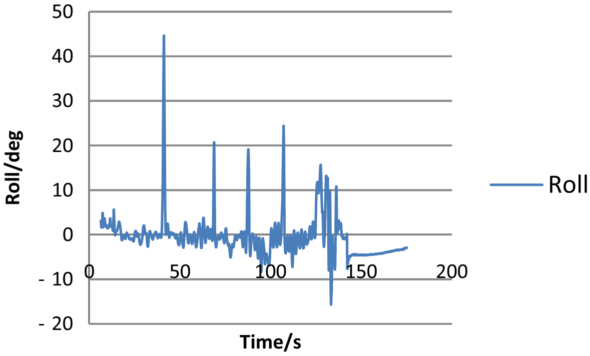

Fig. 42. Roll attitude versus time.

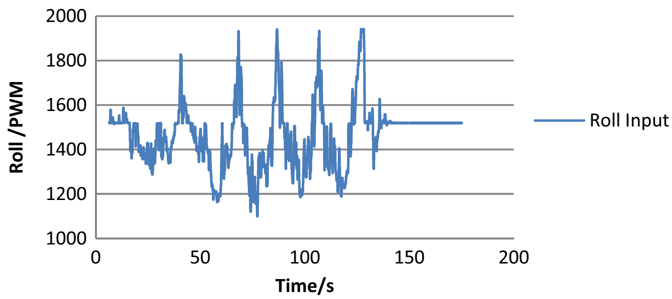

Fig. 43. Roll input versus time.

5.1.1. *Stabilized mode*

Data was collected during stabilized mode and plotted for analysis. Table 9 shows the flight mode the UAV was in at different periods of time.

During forward flight, the ground speed while flying upwind was 8 m/s and while flying downwind was 14 m/s. This equates to airspeed of about 11 m/s with a wind speed of 3 m/s.

The roll attitude and roll input is shown in Figs. 42 and 43, respectively. Comparing the graphs, it can be seen that the UAV is responsive in roll commands.

In Fig. 46, it can be observed that the pitch input and attitude are correlated to a certain extent. Thus, the pitch

Table 9. Flight modes at various times.

Time (s)		Mode
From	To	
6.787	7.73	Hover
7.73	18.73	Transition
18.73	130.68	Cruise
130.68	135.68	Transition
135.68	144.46	Land

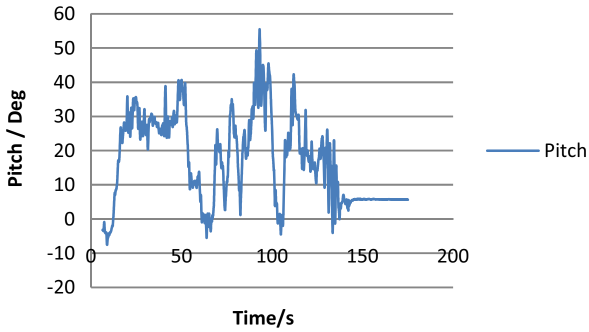

Fig. 44. Pitch attitude versus time.

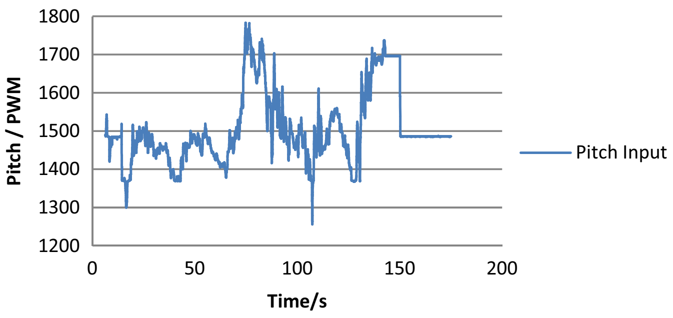

Fig. 45. Pitch input versus time.

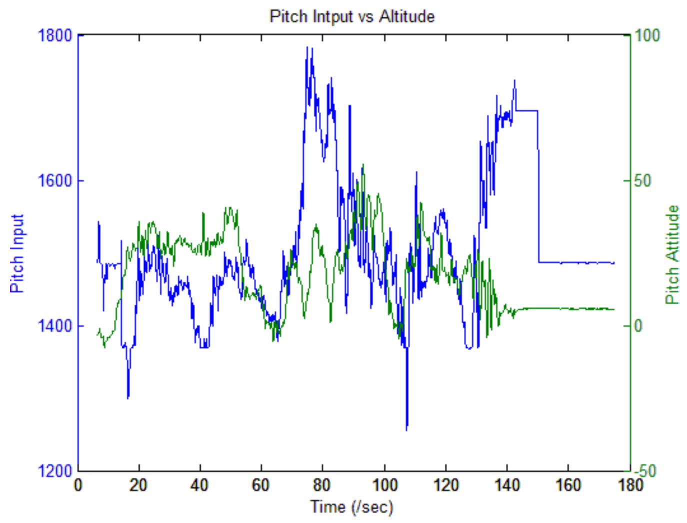

Fig. 46. Comparison of pitch input and pitch attitude.

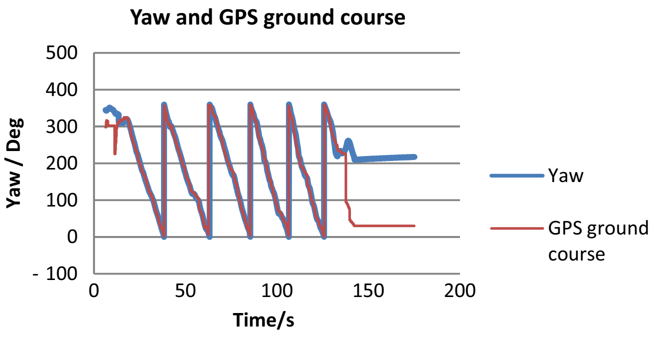

Fig. 47. Yaw data and ground course versus time.

attitude variation is due to user input and not inherent oscillation in the pitch axis.

In Fig. 47, it can be observed that the yaw attitude and the GPS ground course matches. This shows that the yaw attitude measured by the IMU is very similar to the ground course obtained by GPS data, confirming the magnetometer's reliability. An advantage of heading data over GPS ground course is the ability to detect small changes over a short period of time.

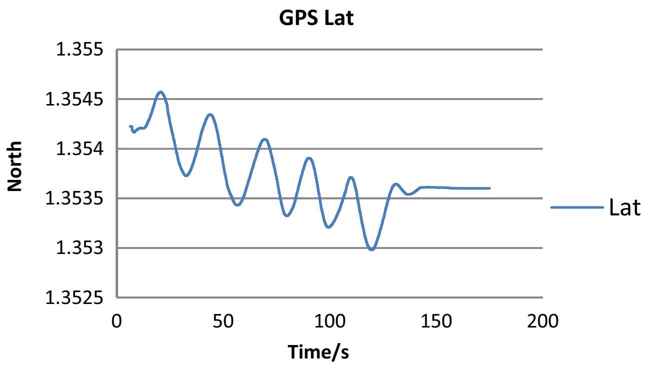

Fig. 48. GPS latitude versus time.

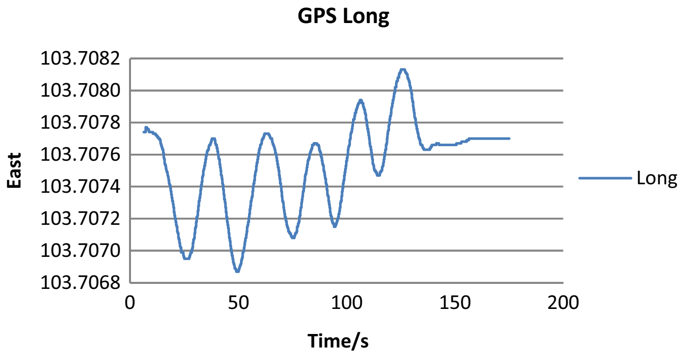

Fig. 49. GPS longitude versus time.

The GPS latitude and longitude data were plotted separately in Figs. 48 and 49. The periodic oscillation shows the UAV circling with its center of circulation shifting southwards. The flight path is shown in Fig. 50.

5.1.2. *Autonomous mode*

While autonomous navigation for hover mode is obtained from open source codes, the autonomous navigation for forward flight was coded. In order to verify the functionality of the code, a flight test was conducted.

The user interface used for forward flight mode is similar to the hover mode. For the first test, four waypoints were planted in for corners of NTU rugby field. In Fig. 51, the waypoints are shown in green while the flight path is shown in yellow.

Figure 52 shows the live telemetry log obtained from the fight test. According to the meteorological station, there was a sustained 20 km/h wind in the northward direction. On the ground, the anemometer measured 7 m/s (25.2 km/h) in the northward direction.

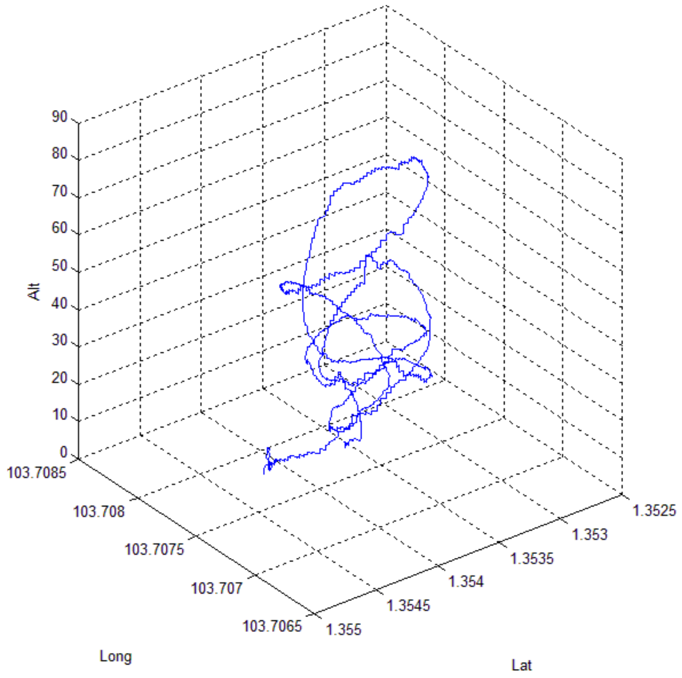

Fig. 50. GPS longitude versus latitude versus altitude.

The flight path is shown in blue and the UAV was able to navigate to all four predetermined waypoints. It can be observed that from waypoint 2 to waypoint 3, when the UAV is flying toward the wind, the trajectory was not smooth and gave a zigzag path. This is due to PID tuning for navigation during forward flight. The proportional gain was increased for the next flight test.

5.2. *Aerodynamics*

As discussed in the design section, the tandem wing tilt rotor is designed to improve aerodynamic considerations in hover, transition and forward flight.

5.2.1. *Hover — Thrust and power required*

To investigate the effectiveness of tiltable wing tips and variable tilt hover in decreasing download during hover out of ground effect (HOGE), three different setups were tested.

The first setup is the conventional setup with no tiltable wing tips as shown in Fig. 53, the second setup is the tiltable wing tips as shown in Fig. 54, and the last setup is tiltable wing tips hovering at a fuselage angle of 45° as shown in Fig. 55. The UAV hovered in the various set up with the power data and throttle setting being logged.

Comparing nontiltable and tiltable wingtips at 90°, the results show that there is a 15.8% decrease in thrust required and a 40.8% decrease in power required. This shows the effectiveness in decreasing the download by using tiltable wing tips.

Comparing tiltable wingtips at 90° and 45°, there is a 14.2% decrease in thrust required and a 3.6% decrease in power required. This is due to the significant decrease in download in the 45° configuration as the fountain effect will be greatly reduced due to the sloping wing.

From this experiment, tiltable wingtips serves as an effective solution to reduce download during HOGE, saving energy and increasing payload capacity. In addition, the

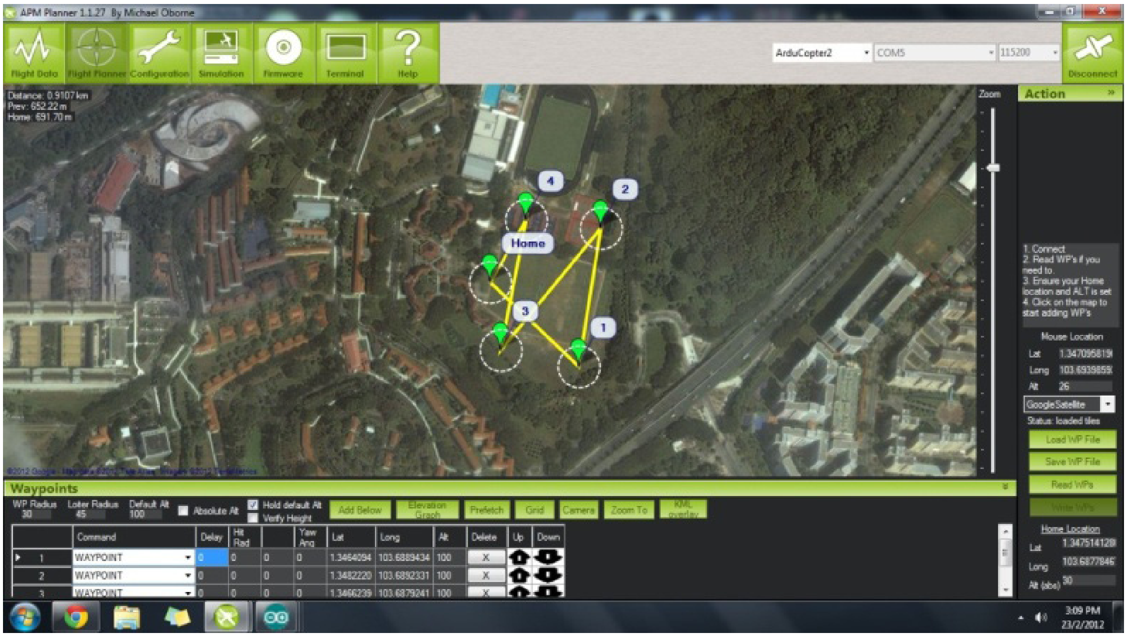

Fig. 51. (Color online) Navigation commands to mission planner.

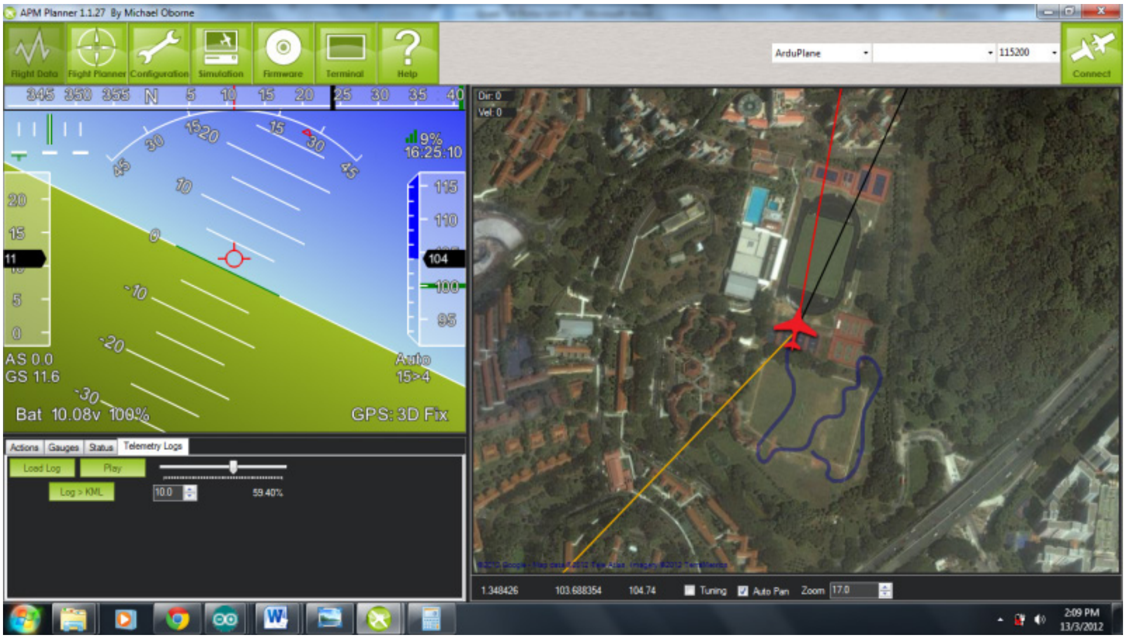

Fig. 52. (Color online) Flight test telemetry log.

Fig. 53. Conventional setup with no tiltable wing tips.

Fig. 54. Setup with tiltable wing tips.

Table 10. Thrust and power required for three different configurations.

	Nontiltable Wingtips	Tiltable Wingtips	
	90° Hover	90° Hover	45° Hover
Thrust required	2400 g	2022 g	1734 g
Power required	370.2 W	219.1 W	211.2 W

variable tilt feature successfully proves to further reduce the thrust and power required.

5.3. *Transition*

The changes in forces and moments calculated during transition were evaluated through two experiments.

First, the net moment from the motors was determined using the test rig. While pivoted about the CG in forward

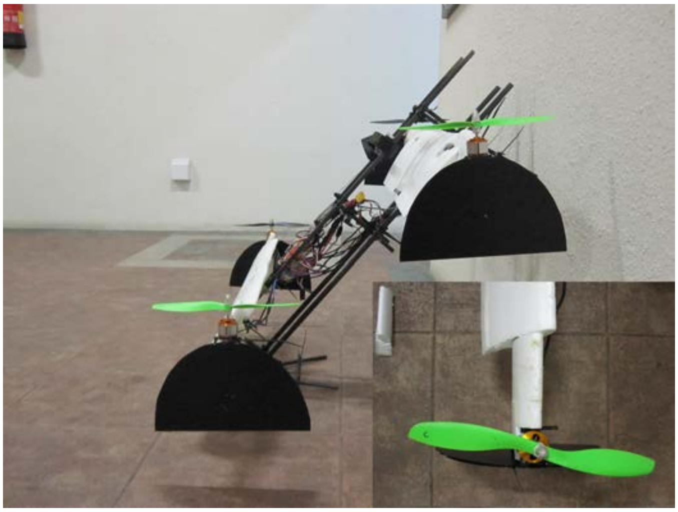

Fig. 55. 45° hover with tiltable wings.

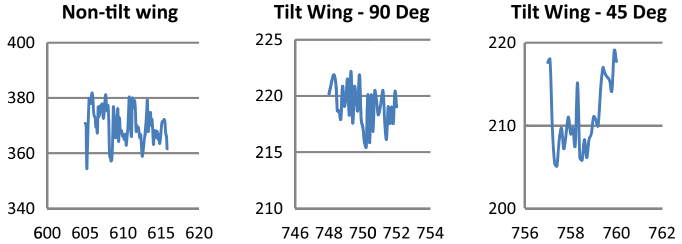

Fig. 56. Power versus time for three different configurations.

flight mode, a mass balance is placed at the nose, 0.35 m from the CG point. A reading of 0.12 kg was measured. The moments were compared with the theoretical calculations.

$$0.35\,\text{m} \times 0.12\,\text{kg} \times 9.81\,\text{m/s}^2 = 0.412\,\text{Nm}.$$

Second, the pitch attitude was logged during transition and the trend follows the dynamic model closely as shown in Figs. 57 and 58. In the first 45°, where the UAV was still in quadcopter mode, there is slight oscillation as it tries to stabilize while tilting. After 45°, the UAV was in plane mode and gradually increase pitch to increase the angle of attack.

The slight increase in pitch attitude can be observed from the snapshots of the flight test during transition.

Table 11. Differences between measurement and dynamic model.

	Measurement	Dynamic Model	Difference
Moments from motor	0.412 Nm	0.475 Nm	15%

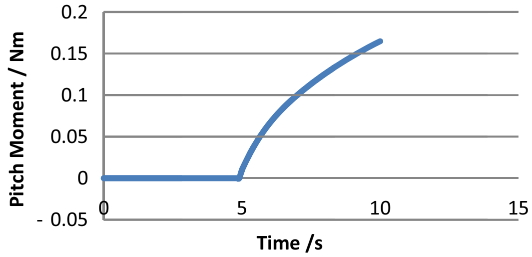

Fig. 57. Pitch moment calculated from dynamic model.

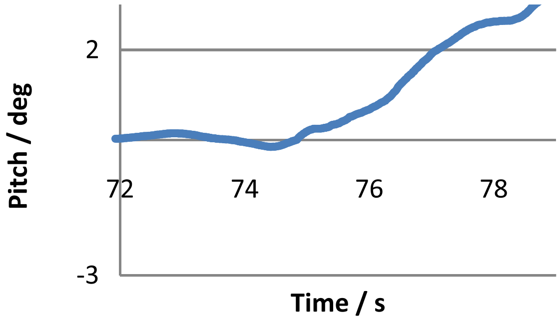

Fig. 58. Pitch attitude obtained from flight test data.

5.4. *Forward flight*

Lift and drag coefficient can be calculated with the formula below using the flight test data.

$$C_D = \frac{F_D}{\frac{1}{2}\rho v^2 A'} \tag{6}$$

$$C_L = \frac{F_L}{\frac{1}{2}\rho v^2 A'} \tag{7}$$

where $F_D = T = 6.75\,\text{N}$

$$\begin{aligned} F_L &= W = 14.72\,\text{N}, \\ \rho &= 1.225\,\text{kg/m}^3, \\ v &= 11\,\text{m/s}, \\ A &= 0.3214\,\text{m}^2, \\ C_D &= \frac{F_D}{\frac{1}{2}\rho v^2 A} = 0.308, \\ C_L &= \frac{F_L}{\frac{1}{2}\rho v^2 A} = 0.673, \\ \frac{C_L}{C_D} &= \frac{0.612}{0.264} = 2.19. \end{aligned}$$

The L/D ratio of the prototype was poor in comparison with other aircrafts. This is due to the open fuselage in the prototype, creating drag and disrupting airflow. The coefficient of lift is less, and coefficient of drag is more than

Fig. 59. Snap shots of transition at various tilt angles.

Table 12. Comparison between aircrafts and L/D.

Aircraft	Scenario	L/D
Boeing 747	Cruise	17
Cessna 150	Cruise	7
Concorde	Approach	4.35

Table 13. Differences between theoretical calculation and experimental result.

	Theoretical calculation	Experiment	Difference
Coefficient of lift	0.81	0.673	16.9%
Coefficient of drag	0.281	0.308	9.6%

the theoretical calculations as the calculations are based on a closed fuselage. In addition, drag from landing gear and exposed wires were not taken into account during calculations.

6. Conclusion

The autonomous tandem wing quad tilt rotor has been successfully designed, developed and tested. The UAV is designed around the requirement of autonomous vertical take-off and landing and efficient forward flight. Additional capabilities to perch and stare are also required.

The first step is to review and investigate current tilt rotor and tandem wings to identify current problem and challenges. Some main problems of current tilt rotors are vortex ring state and download. Vortex right state causes sudden loss of lift during rapid decent, which is an operational requirement that tilt rotors are designed for. Download can account for up to 9% of the thrust produced due to fountain effect, reducing payload capacity and efficiency in HOGE. Interference between wings of tandem wings is investigated in order to optimize the advantages of tandem wing design.

The design process critically investigates aspects including aerodynamics, flight mechanics, structure, electronic system and autopilot. For aerodynamics, two mathematical models were developed to study tiltable wings to reduce download and rear wing elevation for minimal propeller-wing interaction. In flight mechanics, two mathematical models were developed to study the fastest tilt rate for smooth transition and changes in moments during transition. In structure, the light weight yet rigid requirements were considered and the tilt mechanisms were developed. Ardupilot Mega was chosen for the autopilot and the algorithm was modified to incorporate transition and forward flight controls and navigation.

The design was successfully implemented with six variations of the tandem quad tilt rotor. The first three versions were two large outdoor versions and a small indoor version. The third version was to study the use of the tiltable wings as control surfaces instead of ailerons and elevators. The last two versions are developed through optimization and improvements from the previous three models and are used for a competition in USA, organized by DARPA.

Numerous flight tests were conducted, including manual mode, autonomous modes and variable hover mode. A wide range of useful data was collected to evaluate the UAVs. Data logs include PWM outputs, attitudes, GPS, and power data. The data collected is used in comparison with dynamic models and mathematical models, further confirming the effectiveness of those models.

Acknowledgments

The author likes to thank his supervisor, Dr Yongki Go Tiauw Hiong for his guidance during the course of this project.

The author also likes to extend his gratitude to his peers who supported and helped in the flight trials. Special thanks goes to Miss Lim Ming Rong Eunice.

The author wishes to acknowledge the funding support for this project from Nanyang Technological University.

References

[1] Y. Jung, D. H. Shim and N. Ananthkrishnan, Controller synthesis and application to hover-to-cruise transition flight of a tail sitter UAV, KAIST, Daejeon, Republic of Korea, August 2010, pp. 305–701.

[2] C. Meyer, Why tiltrotors fail (2008), www.G2mil.com.

[3] G. Lee, V-22 Osprey: Wonder weapon or widow maker, Center for Defense Information (2006).

[4] W. F. Chana and T. M. Sullivan, Download — The tilt rotor's downfall (AIAA, 1993).

[5] A. Radhakrishnan and F. H. Schmitz, Quad tilt rotor download and power measurements in ground effect (AIAA, 2006).

[6] I. Fejtek and L. Roberts, Navier-Stokes computation of wing leading edge tangential blowing for a tilt rotor in hover (AIAA, 1992).

[7] J. Rutherford, S. Bass, M. Lovenguth and M. D. H. Company, Advance technology tilt wing study (AIAA, 1992).

[8] U. A. Force, Joint Future Theater Lift (JFTL) Technology Study (JTS) (2010).

[9] B. Helicopter, *EagleEye Pocket Guide* (2005).

[10] J. Rutherford, S. Bass, M. Lovenguth and M. D. H. Company, A concept mission sensitivity study of several medium to high-speed V/Stol aircraft (AIAA, 1991).

[11] Y. Xili, F. Yong and Z. Jihong, Transition flight control of two vertical/short takeoff and landing aircraft, *J. Guidance, Control, Dyn* **31**(2) (2008) 15.

[12] O.Soykasap and D. H. Hodges, Aeroelastic optimization of a composite tilt rotor (AIAA, 1998).

[13] I. Fejtek and L. Roberts, Navier-Stokes computation of wing/rotor interaction for a tilt rotor in hover (AIAA, 1991).

[14] D. Casalino, M. Gentito and A. Visingardi, Numerical analysis of noise scattering effects due to the airframe in tilt rotor systems (AIAA, 2006).

[15] T. McGree and I. Kroo, A fundamental comparison of canard and conventional configurations, *J. Aircraft* **20**(11) (1983).

[16] W. Calarese, Closed coupled canard–wing vortex interaction, *J. Aircraft* **21**(2) (1984).

[17] Z. Husain, M. Z. Abdullah and T. C. Yap, Two-dimensional analysis of tandem/staggered airfoils using computational fluid dynamics (2002).

[18] B. Kuhlman, *Radio Control Soaring Digest* **25**(2) (2002) 52.

[19] R. Nelson, *Flight Stability and Automatic Control*, 2nd edn. (McGraw-Hill Ryerson, Limited, 1997).

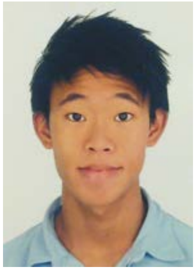

Joshua Jang En Chao received his B.Eng (Aerospace) from Nanyang Technological University in 2012. During his undergrad studies, he was awarded the Nanyang Scholarship and was enrolled into the CN Yang Scholars Programme. He founded the NTU Aeromodelling Club in 2010 and was Vice President of NTU Aerospace Society from 2010 to 2011. In 2011, he led a team of four to participate in Taiwan Unmanned Aircraft Design Competition and clinched first place in Navigated Flight Group Category. Mr Chao co-founded a UAV Startup, Avetics Pte Ltd in 2011 and won the Ideas Inc. Business Challenge 2011, Most Technologically Driven Startup Award. He has been working at DSO National Laboratories since 2012. He is the advisor of Nanyang Technological University Uavionics Society since 2013.